Finite-size scaling study of a lattice-gas model for oxygen chemisorbed on tungsten

P. A. Rikvold,* K. Kaski,† and J. D. Gunton
Physics Department, Temple University, Philadelphia, Pennsylvania 19122

M. C. Yalabik
Physics Department, Middle East Technical University, Ankara, Turkey
(Received 22 November 1983)

We present a finite-size scaling study of a centered rectangular lattice-gas model with attractive nearest-neighbor interactions and repulsive second- and third-neighbor and three-particle interactions, as well as attractive fifth-neighbor interactions. This has been proposed as a model for atomic oxygen adsorbed on a (110) surface of tungsten. The ordered phases are a (2×1) phase with coverage $\frac{1}{2}$ and a (2×2) phase with coverage $\frac{3}{4}$. We obtain phase diagrams which are in good qualitative agreement with the available experimental information. This agreement is obtained with considerably weaker attractive fifth-neighbor interactions than previously suggested by ground-state and Monte Carlo calculations, but consistent with the results of quantum-mechanical band calculations. In particular, we find a multicritical point below which the low-coverage (2×1)-to-disorder transition is of first order. We also find indications of a previously undetected low-temperature multicritical point below which the high-coverage (2×2)-to-disorder transition may be of first order. The finite-size effects in this study are considerably stronger than in previous studies of simpler lattice-gas models. This limits the accuracy with which we can determine the multicritical temperatures. It also prevents us from obtaining reliable estimates of the nonuniversal critical exponents for this model.

I. INTRODUCTION

Recently a number of experimental studies have been aimed at determining the phase diagrams of gases chemisorbed on metal surfaces.[1–4] The observed phase diagrams are rather complicated and quite interesting. It seems clear, for example, that chemisorbed systems provide physical examples of two-dimensional systems exhibiting multicritical points and multiphase coexistence. A schematic representation of the experimental phase diagram for atomic oxygen chemisorbed on a (110) surface of tungsten [O/W(110)] is shown in Fig. 1. The figure is based on data from low-energy electron diffraction[3] (LEED) and surface reflectance spectroscopy (SRS).[4]

It is believed that when surface reconstruction is either absent or simply results in a renormalization of the interaction energies, chemisorbed systems can be described by lattice-gas models.[5,6] The O/W(110) system is thought to fulfill these requirements. However, since the lattice-gas models which we discuss here do not include multilayer adsorption, they can only be expected to accurately represent chemisorbed systems at relatively low coverages. It is also possible that the interaction constants in real systems may depend on the coverage. These limitations notwithstanding, the results from Monte Carlo simulations[7] indicate that lattice-gas models often are adequate to explain the essential features of the phase diagrams for chemisorbed systems.

In order to estimate interaction constants which reproduce the experimentally known features of the O/W(110) phase diagram, we have used the well-known finite-size scaling method[8] to study a lattice-gas model which is thought to describe the phase transitions exhibited by this system. We have obtained phase diagrams which are in good qualitative agreement with the limited experimental information available. We expect that the set of interaction constants which produces these phase diagrams gives reasonable estimates of the interaction energies in the real system.

The finite-size effects in this calculation are, however, considerably larger than those seen in earlier calculations for simpler systems,[9] including previous work on a simplified model for O/W(110).[10] This particularly affects the calculations of critical exponents, which are expected to be nonuniversal for the model studied here. For the spe-

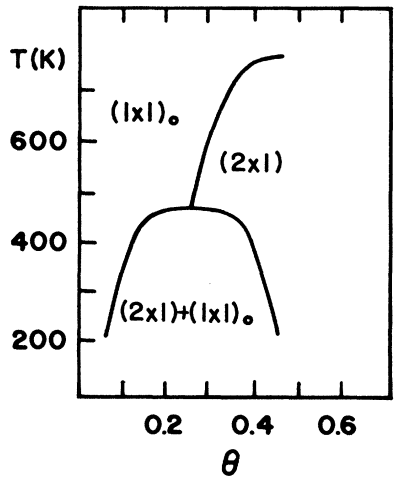

FIG. 1. Schematic sketch of the phase diagram for O/W(110). The figure is based on LEED data from Ref. 3 and SRS data from Ref. 4.

cial choice of interaction constants which allows us to compare our estimates for the critical exponents with those obtained in Ref. 10, the agreement is very poor. This leads us to believe that our exponent estimates are rather unreliable. For this reason we do not discuss them in detail here.[11] The major achievement of the present work is therefore the determination of the phase diagrams.

II. MODEL

The model we have chosen to study is a centered rectangular lattice-gas with competing interactions, which has previously been proposed as a model for the O/W(110) system by Ching *et al.*[7] This model has attractive nearest-neighbor interactions and repulsive second-neighbor, third-neighbor, and three-particle interactions, as well as attractive fifth-neighbor interactions. The centered rectangular lattice corresponding to a W(110) surface, with these interactions indicated, is shown in Fig. 2(a). Estimates for the interaction strengths have been obtained from a combination of ground-state calculations and Monte Carlo simulations of the structure factor, which is proportional to the LEED line intensity.[7] Quantum-mechanical band calculations of the interaction strengths have been reported by Einstein.[12]

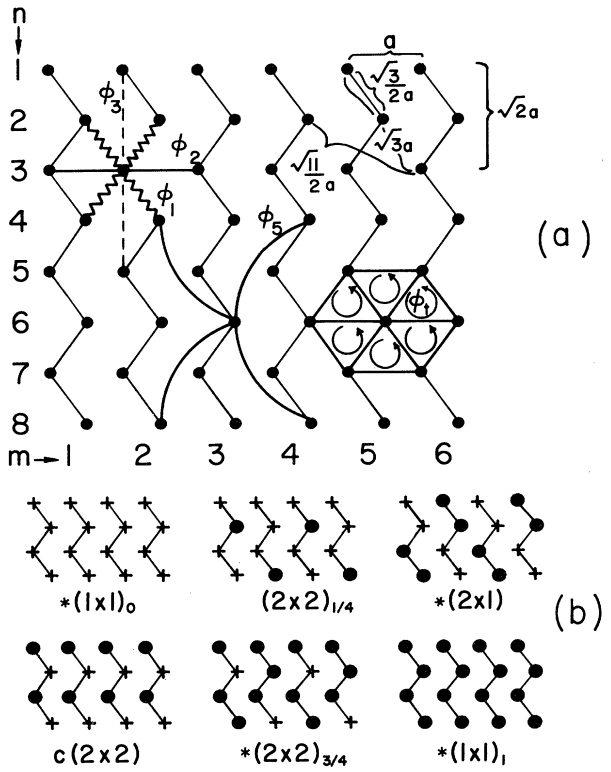

FIG. 2. (a) Centered rectangular lattice corresponding to a (110) surface of a body-centered cubic lattice with lattice constant a. The zigzag-shaped layers into which the lattice is decomposed for transfer-matrix calculations are indicated by light lines. The index m denotes the layers, and the index n numbers the individual sites within each layer. In the upper right-hand corner of the figure are indicated the intersite distances up to fifth neighbors. The pairwise and triplet interactions in which a particular lattice site takes part are also indicated. In the upper left-hand corner are shown the nearest-neighbor (ϕ_1), second-neighbor (ϕ_2), and third-neighbor (ϕ_3) interactions around the site ($m=2$, $n=3$). In the lower central part of the figure are shown the fifth-neighbor interactions (ϕ_5) around the site ($m=3$, $n=6$). In the lower right-hand corner are shown the interaction triplets (ϕ_t) surrounding the site ($m=5$, $n=6$). The triplet interactions are not isotropic. (b) The disordered states $(1\times1)_0$ and $(1\times1)_1$, and the ordered states $(2\times2)_{1/4}$, (2×1), $c(2\times2)$, and $(2\times2)_{3/4}$ which can be reached by a second-order phase transition. The subscripts denote the coverage. Those states which can be realized as ground states with the Hamiltonian (2) are indicated by an asterisk.

The observed phase diagrams are not symmetric about the coverage $\Theta=\frac{1}{2}$. Since lattice-gas models with purely pairwise interactions are symmetric under interchange of particles and vacancies, this observed asymmetry necessitates the inclusion of three-particle interactions. The choice of which three-particle interactions to include is not unique, but is based on bond-length considerations. The long axis of the set of interaction triangles surrounding a specific lattice point is chosen parallel to the short side of the conventional rectangular unit cell. The three-particle interactions are thus anisotropic.

The attractive fifth-neighbor interactions lower the energies of all the phases permitted by the lattice symmetry by the same amount,[10] thus encouraging the formation of ordered islands. This effect may introduce phase coexistence and multicritical points. When the fifth-neighbor interactions are absent all phase transitions in the model are expected to be second order. This special case has been studied by Kaski *et al.*,[10] using the finite-size scaling method. The second-order transitions are thought to belong to the universality class of the XY model with cubic anisotropy.[13] The critical exponents therefore are expected to be nonuniversal and to vary with the interaction constants as well as with chemical potential or coverage.

In terms of the local occupation variable c_i, which is 0 or 1 depending on whether the ith site is empty or occupied by an adatom, the coverage Θ is defined as

$$\Theta=N^{-1}\sum_i \langle c_i\rangle \ . \tag{1}$$

Here N is the total number of lattice sites, and the angular brackets denote a thermal average. The model described above is defined in the grand-canonical ensemble by the lattice-gas (LG) Hamiltonian

$$\mathscr{H}_{\mathrm{LG}}-\mu\Theta N=-\phi_1\sum_{\mathrm{NN}}c_ic_j-\phi_2\sum_{\mathrm{2N}}c_ic_j-\phi_3\sum_{\mathrm{3N}}c_ic_j$$
$$-\phi_5\sum_{\mathrm{5N}}c_ic_j-\phi_t\sum_{\Delta}c_ic_jc_k-(\mu+\epsilon)\sum_i c_i \ . \tag{2}$$

Here ϕ_1, ϕ_2, ϕ_3, and ϕ_5 are the nearest-neighbor, second-neighbor, third-neighbor, and fifth-neighbor interactions indicated in Fig. 2(a), respectively. The ϕ_t are the three-particle interactions, also shown in Fig. 2(a). The sums $\sum_{\mathrm{NN}}$, $\sum_{\mathrm{2N}}$, $\sum_{\mathrm{3N}}$, and $\sum_{\mathrm{5N}}$ extend over all nearest-, second-, third-, and fifth-neighbor pairs on the centered rectangular lattice, respectively. The sum $\sum_{\Delta}$ extends

over all triplets connected by the three-particle interaction ϕ_t. The chemical potential and binding energy per site are μ and ϵ, respectively.

As is customary, we transform Eq. (2) to Ising-spin language by taking $c_i=(1-\sigma_i)/2$, where $\sigma_i=\pm 1$, obtaining

$$\mathcal{H}=-J_1\left[\sum_{\mathrm{NN}}\sigma_i\sigma_j+R_2\sum_{\mathrm{2N}}\sigma_i\sigma_j+R_3\sum_{\mathrm{3N}}\sigma_i\sigma_j+R_5\sum_{\mathrm{5N}}\sigma_i\sigma_j+R_t\sum_{\Delta}\sigma_i\sigma_j\sigma_k+H\sum_i\sigma_i\right]. \tag{3}$$

The Ising-model interactions are simply related to those of the lattice-gas formulation.[10] The magnetization M is related to the coverage Θ by $M=1-2\Theta$.

The symmetry of the centered rectangular lattice only permits the following ordered states to be reached via a second-order phase transition: (2×1) or (1×2) with $\Theta=\frac{1}{2}$, $(2\times 2)_{1/4}$ with $\Theta=\frac{1}{4}$, $(2\times 2)_{3/4}$ with $\Theta=\frac{3}{4}$, and $c(2\times 2)$ with $\Theta=\frac{1}{2}$.[13] Further possible ground states are the disordered filled state $(1\times 1)_1$ with $\Theta=1$, and the disordered empty state $(1\times 1)_0$ with $\Theta=0$. These states are shown in Fig. 2(b). Their energies per site are the same as those given in Ref. 10, with the addition of a term $-2R_5$ for each possible ground state, due to the fifth-neighbor interactions. The critical field values which separate the ground states are found by pairwise equating the ground-state energies.[7,10] With the choice of parameters used in this work, namely, $R_2=R_3=-1.0$ and $R_t=1.25$, the ground states and the critical fields are as follows: disordered filled $(1\times 1)_1$ for $H<-7.5$, $(2\times 2)_{3/4}$ for $-7.5<H<-1.5$, (2×1) for $-1.5<H<-0.5$, and disordered empty $(1\times 1)_0$ for $H>-0.5$. Both the ordered ground states are fourfold degenerate. Neither $(2\times 2)_{1/4}$ nor $c(2\times 2)$ are realized as ground states, in agreement with the experimental phase diagrams.

III. CALCULATIONS

The finite-size scaling method and transfer-matrix calculations have been adequately discussed elsewhere.[8,10,14,15] We will, therefore, here only consider its application to the specific model introduced above. We consider a centered rectangular lattice in the form of an infinitely long strip, N sites wide. If the layers are chosen parallel to one of the primitive lattice vectors, the fifth-neighbor interactions connect sites on nonadjacent layers. To avoid this and limit the range of the Hamiltonian to adjacent layers of the lattice, we define zigzag-shaped layers, as shown in Fig. 2. The position of a site is given by the index m, which indicates the layer, and the index n, which numbers the individual sites within each layer. The directions of m (longitudinal) and n (transverse) are shown in Fig. 2(a). Each site is occupied by an Ising spin $\sigma_{m,n}=\pm 1$. The system obeys periodic boundary conditions $\sigma_{m,n}=\sigma_{m,n+N}$.

The ground states are invariant under four-step translations in the n direction, as seen from Fig. 2(b). In order to avoid the introduction of interfaces, the strip width N must therefore be an integral multiple of 4. With $N'=N+4$ the Nightingale condition[8] for the determination of the critical point $\underline{K}_c$ becomes

$$\frac{\xi_N(\underline{K}_c)}{N}=\frac{\xi_{N+4}(\underline{K}_c)}{N+4}, \tag{4}$$

where $\xi_N(\underline{K})$ is the correlation length. The symbol $\underline{K}$ denotes the set of nonordering fields, $\underline{K}=(T,H)$. For the method to be of any use, these finite-size estimates for $\underline{K}_c$ must converge rapidly to their infinite-system value. This appears to be the case in most previous applications of the method.[8,10,15] For the rather complicated model we are studying here, we have not been able to obtain a sufficiently large range of strip widths to actually test the convergence, except at low temperatures, where it indeed seems to be fast. Earlier experience with a simpler model[15] also indicates that the condition (4) can be used to locate a first-order transition point quite accurately.[16]

The correlation length ξ_N is obtained from the two largest eigenvalues λ_1 and λ_2 of the transfer matrix by[8,14]

$$\xi_N=\left[\ln\frac{\lambda_1^{(N)}}{|\lambda_2^{(N)}|}\right]^{-1}, \tag{5}$$

and the transfer matrix $\underline{\underline{T}}$ is defined by its elements

$$\langle S_m|\underline{\underline{T}}|S_{m+1}\rangle=e^{-\beta\mathcal{H}_m(S_m,S_{m+1})}. \tag{6}$$

Here S_m denotes the Ising-spin configuration of the mth layer. To obtain $\underline{\underline{T}}$ explicitly we decompose the Hamiltonian $\mathcal{H}$ into a sum of single-layer contributions,

$$\mathcal{H}=\sum_{m=1}^{\infty}\mathcal{H}_m(S_m,S_{m+1}). \tag{7}$$

We do not explicitly give $\mathcal{H}_m$ here.[11]

The transfer matrix defined by $\mathcal{H}_m$ is not symmetric under matrix transposition, due to the nearest-neighbor and three-body terms. A generalization of the transfer-matrix formalism necessary to handle this case can be given.[11] The eigenvalues of the nonsymmetric $\underline{\underline{T}}$ are either real or occur in complex-conjugate pairs, $\lambda_{\gamma\pm}=|\lambda_\gamma|e^{\pm i\phi_\gamma}$. The angle ϕ_γ gives the periodicity in the m direction of a state built from the eigenvectors $|\gamma+\rangle$ and $|\gamma-\rangle$, and the complex-conjugate pair contributes *one single* length scale $(\ln|\lambda_1/\lambda_\gamma|)^{-1}$ to the correlation function. As in the case of a symmetric $\underline{\underline{T}}$, the largest eigenvalue λ_1 is always positive and nondegenerate by virtue of the Perron-Frobenius theorem.[14] Although there are no fundamental difficulties associated with handling a model defined by a nonsymmetric transfer matrix, it roughly doubles the computer storage and time requirements, as compared to the case of a symmetric $\underline{\underline{T}}$. This makes it more difficult to attain large strip widths.

The centered rectangular lattice and the Hamiltonian $\mathcal{H}$ both are invariant under a two-step translation in the n direction, but not under a one-step translation. We have block diagonalized $\underline{\underline{T}}$ with this two-step translation, as described in the Appendix. The order parameters can be decomposed into linear combinations of single-layer order parameters, as discussed in the Appendix. The single-layer order parameters,

$$\psi_{(2\times1)}(m)=\frac{1}{N}\sum_{p=1}^{N/2}(-1)^p(\sigma_{m,2p-1}-\sigma_{m,2p}) \tag{8a}$$

and

$$\psi_{(1\times2)}(m)=\frac{1}{N}\sum_{p=1}^{N/2}(-1)^{p-1}(\sigma_{m,2p-1}+\sigma_{m,2p}) , \tag{8b}$$

which describe the ordered phases, are antisymmetric under the two-step translation operation. The single-layer order parameter

$$\psi_{\mathrm{FM}}(m)=\frac{1}{N}\sum_{p=1}^{N}\sigma_{m,n} , \tag{9}$$

which characterizes the disordered phases, is symmetric under the same operation. In order to find the leading length scales of the order-parameter correlation functions, we therefore need only to diagonalize the symmetric and antisymmetric blocks of $\underline{\underline{T}}$. In contrast to the dimension 2^N of the full transfer matrix, the dimension of the symmetric block is 10 for $N=4$, 70 for $N=8$, and 700 for $N=12$. The symmetric and antisymmetric block of $\underline{\underline{T}}$ may be further block diagonalized by utilizing the reflection symmetry of $\mathscr{H}$ about $n=N/2$. We have not, however, implemented this reduction here.

For the strip width $N=8$ the block diagonalization described above reduces the dimension of the transfer matrix sufficiently that it can easily be numerically diagonalized. To handle the case of $N=12$ we have developed a truncation scheme for the transfer matrix, based on first-order perturbation theory.[11] This allows us to obtain the correlation length with a given absolute accuracy. If the dimension of the truncated matrix required to attain this accuracy exceeds 172, the matrix is truncated at this size, and the resulting accuracy is estimated. This truncation procedure gives good results at low temperatures. At high temperatures, where the eigenvalue spectrum becomes very densely spaced, however, the accuracy is considerably poorer. Therefore we have only determined the high-temperature parts of the phase diagrams from scaling with $N/N'=4/8$.

At the multicritical points the disordered phase and the fourfold-degenerate ordered phase become indistinguishable.[17,18] In a manner entirely analogous to the tricritical case studied in Ref. 15, this requires the asymptotic degeneracy of the five largest eigenvalues of the transfer matrix. The two largest eigenvalues of the antisymmetric block of $\underline{\underline{T}}$, corresponding to the two antisymmetric eigenstates which can be formed from the ordered states, are, in fact, exactly degenerate. These two eigenstates have opposite parity under reflection about $n=N/2$. In finite systems the asymptotic degeneracy is evident as a linear divergence with the strip width N of the length scales $[\ln(\lambda_1/|\lambda_i|)]^{-1}$ for $i=1,\ldots,4$. (As mentioned above, the exactly degenerate eigenvalue contributes only one single length scale.) As our numerical criterion for determining a multicritical point, we have chosen to use the linear divergence of the second correlation length[15] $\hat{\xi}_N=[\ln(\lambda_1/|\lambda_3|)]^{-1}$. Thus at the multicritical temperature $T=T_m$,

$$\hat{\xi}_N\approx A_m N \quad \text{as } N\to\infty . \tag{10}$$

In different regions of the phase diagram λ_3 is the second largest eigenvalue of the symmetric block, or the doubly degenerate largest eigenvalue of the antisymmetric block. In the latter case $\hat{\xi}_N$ is the leading length scale of the order-parameter correlation function, whereas in the former case it is the leading length scale of the correlation function for the local coverage. This follows from the discussion in the Appendix. The exact ordering of the largest eigenvalues appears to be strongly dependent on the system size.

Along the line of critical points the susceptibility remains finite as $N\to\infty$, so for $T>T_m$ the characteristic length $\hat{\xi}_N$ must be asymptotically independent of N,

$$\hat{\xi}_N\approx A_2 \quad \text{as } N\to\infty . \tag{11}$$

The behavior of $\hat{\xi}_N$ along the line of first-order transitions below the multicritical point can be obtained from the following argument. At a first-order transition in a semi-infinite system, phase coherence extends over distances which are much larger than the strip width N. The distinct coexisting phases form a quasi-one-dimensional array of single-phase domains.[16,19,20] The ratios of the length scales describing the domains of the different phases are determined by the fractions of the total volume that they occupy, so that $\hat{\xi}_N$ should be proportional to the correlation length ξ_N. The domain size in the longitudinal direction is limited only by surface-tension effects. The free energy of an interface cutting across the system is approximately $N^{d-1}T\sigma(T,H)$, where $T\sigma(T,H)$ is the surface tension of the interface. The asymptotic behavior of $\hat{\xi}_N$ is therefore given by

$$\hat{\xi}_N\approx\hat{D}_N(T,H)e^{N^{d-1}\sigma(T,H)} \quad \text{as } N\to\infty . \tag{12}$$

The asymptotic relations (10)—(12) yield the following criterion for estimating the multicritical temperature T_m:

$$\Delta_{N/N'}\equiv\frac{\hat{\xi}_N}{N}-\frac{\hat{\xi}_{N+4}}{N+4}\begin{cases}>0 & \text{for } T>T_m\\ =0 & \text{for } T=T_m\\ <0 & \text{for } T<T_m .\end{cases} \tag{13}$$

To improve this estimate in the manner discussed in Ref. 15 where the regular part of $\hat{\xi}_N$ as well as corrections to scaling due to irrelevant variables were taken into account, would require data for at least four different strip widths, i.e., for $N=4$, 8, 12, and 16. Obtaining data for $N=16$ or 20 would require extremely large computer resources, even if the dimension of the transfer matrices were reduced as much as possible by symmetry considerations and the eigenvalue routines were specifically designed for the particular problem. The accuracy with which multicritical temperatures can be determined by finite-size scaling methods in systems as complicated as the one we are studying here is therefore rather limited.

IV. RESULTS

We have determined phase diagrams by finite-size scaling with $N/N'=4/8$ for interaction constants $J_1>0$, $R_2=R_3=-1.0$, $R_t=1.25$, and $R_5=0$ and 0.25. For the same set of short-range interactions, and $R_5=0.01$, we

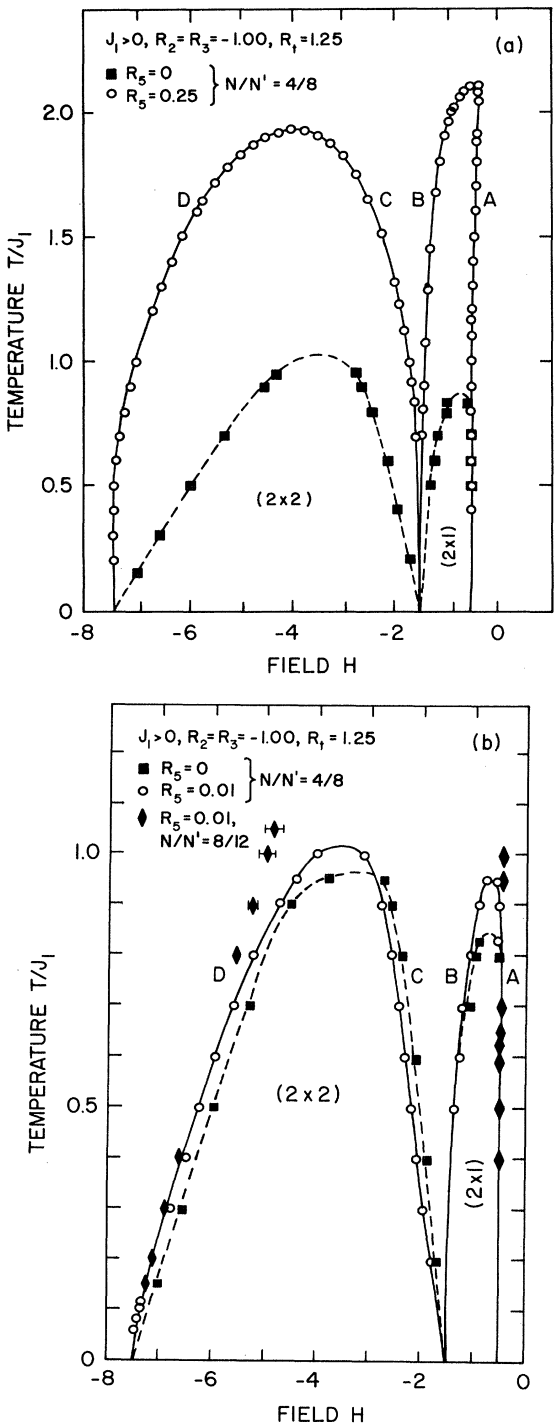

FIG. 3. Phase diagrams in the H-T plane (Ising-model representation) for attractive nearest-neighbor interaction ($J_1>0$) and repulsive second-neighbor, third-neighbor, and triplet interactions ($R_2=R_3=-1.00$, $R_t=1.25$). A: (2×1)-to-$(1\times1)_0$ transition lines; B: (2×1)-to-disorder transition lines; C: (2×2)-to-disorder transition lines; D: (2×2)-to-$(1\times1)_1$ transition lines. (a) Squares and dashed line: $R_5=0$; Circles and solid line: $R_5=0.25$. All calculations were performed with $N/N'=4/8$. (b) Squares and dashed line: $R_5=0$; Circles and solid line: $R_5=0.01$. Both calculated with $N/N'=4/8$. Diamonds with error bars: $R_5=0.01$, $N/N'=8/12$. The data for $N/N'=8/12$ become unreliable at high temperatures due to truncation errors in the $N=12$ transfer matrix.

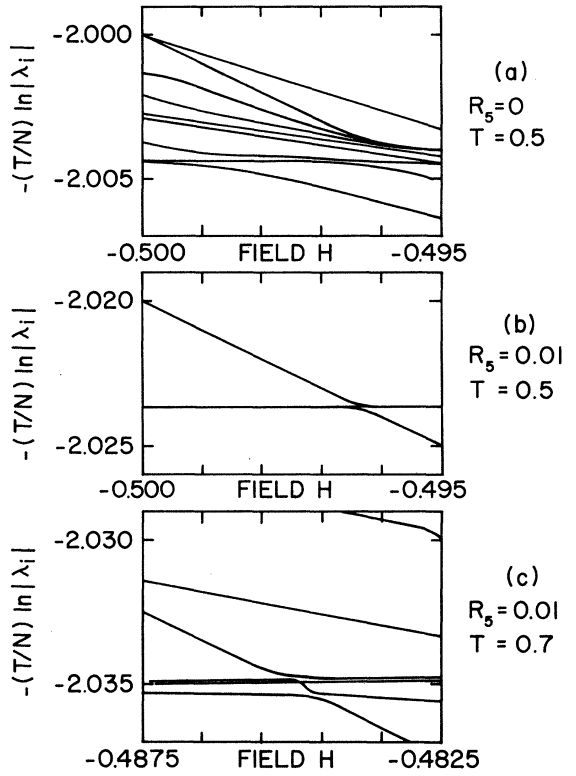

FIG. 4. $g_i(T,H)=-(T/N)\ln|\lambda_i|$ for the largest eigenvalues λ_i as functions of field across the (2×1)-to-$(1\times1)_0$ transition line (A). Strip width $N=12$. The branch $g_1(T,H)$, corresponding to the largest eigenvalue λ_1 is the Gibbs free energy per site. (a) $R_5=0$, $T=0.5$; second-order transition. (b) $R_5=0.01$, $T=0.5$; first-order transition. (c) $R_5=0.01$, $T=0.7$; second-order transition.

have also used $N/N'=8/12$. The value $R_5=0.25$ is consistent with the estimates from ground-state and Monte Carlo calculations.[7] The value $R_5=0.01$ is consistent with quantum-mechanical calculations,[12] which yield that the envelope of the interaction constants varies as (distance)$^{-5}$. The value $R_5=0$ corresponds to the simplified model with only short-range interactions, previously studied by Kaski *et al.*[10] The resulting phase diagrams in the H-T plane for $R_5=0.25$ and $R_5=0$ are shown in Fig. 3(a), and for $R_5=0.01$ and $R_5=0$ in Fig. 3(b).

The phase diagrams are seen to be quite sensitive to the value of the fifth-neighbor interaction constant R_5. For $R_5=0.01$ the maximum critical temperature of the (2×2) phase is about 5% higher than for $R_5=0$, and the maximum critical temperature of the (2×1) phase is increased by about 13%. This reflects the effects of the attractive fifth-neighbor interactions on the eigenvalue spectrum. The gap between the largest eigenvalues, which approximately correspond to the ground states, and the smaller eigenvalues corresponding to excited states, increases dramatically even for very small R_5. This effect is accompanied by a decrease in the spacings between the almost degenerate largest eigenvalues. These effects are illustrated in Fig. 4, which shows the quantities $g_i(T,H)=-(T/N)\ln|\lambda_i|$ for the largest eigenvalues of

T as H is varied across the (2×1)-to-$(1\times1)_0$ transition line which is marked A in Fig. 3(b). The data are for $N=12$. The Gibbs free energy per site is $g_1(T,H)$, corresponding to the largest eigenvalue λ_1. Eigenvalue spectra for $R_5=0$ and 0.01 at $T=0.5$ are shown in Figs. 4(a) and 4(b), respectively. The spectrum for $R_5=0.01$ at $T=0.7$ is shown in Fig. 4(c). For $R_5=0.25$ the effects are even more dramatic and seem to cause the (2×1)-to-$(1\times1)_0$ transition to be of first order along the entire line A. We therefore conclude that $R_5=0.25$ is too strong to yield phase diagrams in agreement with experiments.

In the case of vanishing fifth-neighbor interactions the net interaction between adatoms is repulsive and does not favor island formation. Hence all the phase transitions are second order in this case, as has been verified in the earlier study by Kaski *et al.*[10] The phase diagram for $R_5=0$, presented in Fig. 3, is in good agreement with this earlier study, in which the centered rectangular lattice was decomposed into layers parallel to one of the primitive lattice vectors. We believe the quantitative differences of a few percent are finite-size effects that are related to the decomposition of the lattice into zigzag-shaped layers, used in the present study.

In order to determine the multicritical points for the case of $R_5=0.01$ we have calculated $\Delta_{N/N'}$, which was defined in Eq. (13), along the transition lines. The quantities $\Delta_{4/8}$ and $\Delta_{8/12}$ on the (2×1)-to-$(1\times1)_0$ transition line (A) are shown as functions of temperature in Fig. 5(a). They are seen to vanish at a temperature $T_{m0}/J_1=0.60\pm0.05$, which we interpret as corresponding to a multicritical point. The eigenvalue spectra for $T/J_1=0.5$, shown in Fig. 4(b), and $T/J_1=0.7$, shown in Fig. 4(c), thus correspond to temperatures slightly below and above the multicritical temperature, respectively. The rapid change in the slope of $g_1(T,H)$ in the first-order case (b) corresponds to a discontinuity in the coverage. An attractive fifth-neighbor interaction constant $R_5=0.01$ is thus sufficiently strong to reproduce the experimentally observed multicritical temperature, which is approximately one-half the maximum critical temperature.

We have also calculated $\Delta_{4/8}$ and $\Delta_{8/12}$ [Eq. (13)] versus temperature along the (2×2)-to-$(1\times1)_1$ transition line, which is marked D in Fig. 3(b), as shown in Fig. 5(b). They both vanish at a temperature $T_{m1}/J_1=0.15\pm0.05$. We interpret this as representing another multicritical point associated with the coexistence between the (2×2) and the $(1\times1)_1$ phases. It is, however, possible that it is a finite-size effect and that the temperature where $\Delta_{N/N'}$ vanishes goes to zero as $N,N'\to\infty$.

The (2×1)-to-disorder and (2×2)-to-disorder transition lines marked B and C, respectively, in Fig. 3(b), were only determined by scaling with $N/N'=4/8$. Along the line B, $\Delta_{4/8}$ is slightly negative both for $R_5=0.01$ and for $R_5=0$. Since the transition is known to be of second order in the latter case we believe that this is a finite-size effect and that the order of the transition is unchanged by the attractive fifth-neighbor interactions. Along the line C, $\Delta_{4/8}$ is positive, as expected for a second-order transition.

The transition lines B and C seem to meet at a third multicritical point at ($T=0$, $H=-1.5$). There is no indication that this multicritical point occurs at a nonzero temperature for the interaction $R_5=0.01$. For $R_5=0.25$ the lines B and C come too close to resolve by scaling with $N/N'=4/8$ at low temperatures. We do, however, believe that this is a finite-size effect, and that the multicritical temperature is zero in this case as well.

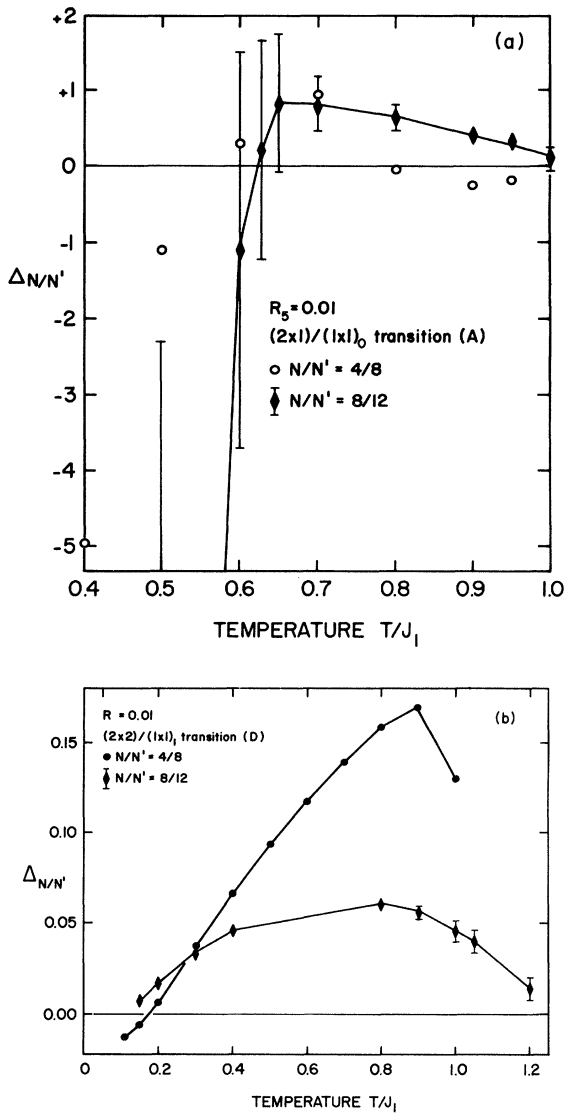

FIG. 5. Quantities $\Delta_{4/8}$ (circles) and $\Delta_{8/12}$ (diamonds with error bars), defined in Eq. (13), for $R_5=0.01$. The error bars indicate the truncation errors in the transfer matrix for $N=12$. (a) Along the (2×1)-to-$(1\times1)_0$ transition line (A). The multicritical temperature is determined from this figure as $T_{m0}=0.60\pm0.05$. (b) Along the (2×2)-to-$(1\times1)_1$ transition line (D). We interpret this figure as indicating a multicritical temperature $T_{m1}=0.15\pm0.05$. It is, however, possible that this is a finite-size effect and that the temperature where $\Delta_{N/N'}$ vanishes goes to zero as $N,N'\to\infty$.

The coverage was computed from the Gibbs free energy per spin as $\Theta=[1+\partial g_1(T,H)/\partial H]/2$. The phase diagrams in the Θ-T plane for $R_5=0$ and 0.01 are shown in Figs. 6(a) and 6(b), respectively. The phase diagram for $R_5=0$ agrees qualitatively with the result obtained by

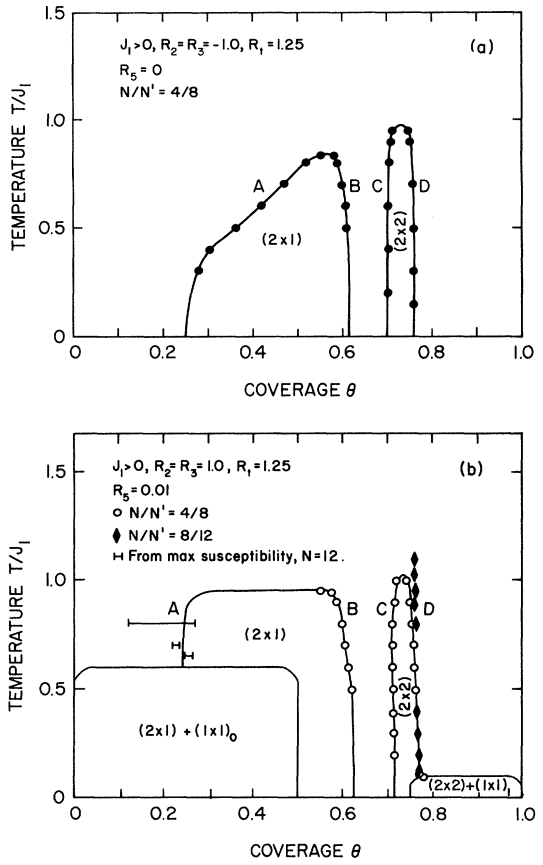

FIG. 6. Phase diagrams in the Θ-T plane (lattice-gas representation) with the same short-range interactions as in the previous figures. (a) $R_5=0$, $N/N'=4/8$. All the transition lines are second order. This phase diagram is in good qualitative agreement with the one obtained in Ref. 10. (b) $R_5=0.01$. $N/N'=4/8$ (circles), $N/N'=8/12$ (diamonds), and coverage at the field corresponding to the maximum susceptibility for $N=12$ (horizontal error bars). The $(2\times1)+(1\times1)_0$ coexistence region for $T<T_{m0}$ and the possible $(2\times2)+(1\times1)_1$ coexistence region for $T<T_{m1}$ are only schematically indicated. The high-temperature portion of the (2×1)-to-$(1\times1)_0$ transition line (A) is merely drawn as a guide to the eye.

Kaski *et al.*[10] We believe that the quantitative differences are finite-size effects due to the different decompositions of the lattice, which were used in these two studies. The coverage has been computed at the transition field obtained from the finite-size scaling condition (4) except on the (2×1)-to-$(1\times1)_0$ transition line A, for $R_5=0.01$. Here the susceptibility peak is so narrow that the coverage evaluated at the finite-size scaling estimate for the transition field, corresponds to the $(1\times1)_0$ phase. Along the second-order portion of this transition line we have, therefore, evaluated Θ at the field corresponding to the maximum susceptibility. Below the multicritical point the peak in the susceptibility is exceedingly sharp, with a half width $\Delta H\lesssim10^{-5}$, and the coverage jumps almost discontinuously from $\Theta\cong0$ to $\Theta\cong\frac{1}{2}$. We therefore only indicate the $(2\times1)+(1\times1)_0$ coexistence region schematically in the Θ-T phase diagram. As well, we have been unable to determine the shape of the possible low-temperature $(2\times2)+(1\times1)_1$ coexistence region, which we therefore also indicate schematically. The low-coverage region of the phase diagram for $R_5=0.01$, shown in Fig. 6(b), is in good agreement with the experimental phase diagram, Fig. 1.

We also have attempted to compute the thermal exponent $\nu=1/y_T$ by differentiation of the correlation length with respect to the field in the manner discussed in Ref. 15. For $R_5=0$ our results are in very poor agreement with those previously obtained by Kaski *et al.*[10] We suggest that this may be a strong finite-size effect related to the nonuniversality of the critical exponents of the present model. We therefore do not attach much significance to our exponent estimates and will not discuss them further here.[11]

V. CONCLUSION

The purpose of this study has been to obtain a set of lattice-gas interaction constants which can reproduce the experimentally known features of the O/W(110) phase diagram. We have found that in a lattice-gas model with attractive nearest-neighbor and repulsive second-neighbor, third-neighbor, and triplet interactions, attractive fifth-neighbor interactions as weak as 1% of the nearest-neighbor interactions are sufficient to introduce pronounced first-order behavior. This model yields phase diagrams which are in good qualitative agreement with those obtained by experiments. This is a much weaker island-forming interaction than had been suggested in previous studies,[7] where the lattice-gas interaction constants have been estimated from ground-state calculations and fitting of the scattering intensities and island shapes obtained in Monte Carlo simulations. These weak fifth-neighbor interactions are, however, consistent with the results of quantum-mechanical band calculations.[12] An additional check on the fifth-neighbor and three-particle interaction constants used in this study would be a determination of the resulting island shapes from Monte Carlo simulations. This is left for future study.

The phase diagram in the H-T plane is easily obtained with an accuracy of a few percent, using strip widths up to $N=12$. The multicritical temperature for the (2×1)-to-$(1\times1)_0$ transition is obtained with an accuracy of about 10%. A more accurate determination of the multicritical points and the phase diagram in the Θ-T plane would require calculations with $N=16$ and possibly $N=20$, which is inaccessible with present-day technology. Nevertheless we find it possible that our results indicate the existence of a previously undetected $(2\times2)+(1\times1)_1$ coexistence region at low temperatures.

Finally we note that in this study the finite-size scaling method yields considerably less accurate results than when it is applied to simpler systems. This is particularly true for the critical-exponent estimates, which we have not discussed in detail here.

ACKNOWLEDGMENTS

This work was supported by grants from National Science Foundation (No. DMR-80-13700), U. S. Office of Naval Research (No. N00014-83-K-0382), and North

Atlantic Treaty Organization (No. RG222.80). One of us (P.A.R.) also acknowledges support from the Norwegian Research Council for Science and the Humanities (Norges Almenvitenskapelige Forskningsråd).

APPENDIX

The transfer matrix $\underline{\underline{T}}$ is an operator on the 2^N-dimensional vector space generated by the single-layer physical configurations $|S\rangle$. If U is another operator which acts on the same space and commutes with $\underline{\underline{T}}$, the latter can be block diagonalized. Each block corresponds to a different eigenvalue of U. Operators U, which correspond to physical transformations of the system such as translations, reflections, or other spin permutations, are unitary. Since the number of states is finite, U is a cyclic transformation whose period L we denote by a subscript, U_L. The period L is also the number of distinct eigenvalues of U_L. For most systems, the only transformations which commute with $\underline{\underline{T}}$ are translations and reflections. Since reflections have only two eigenvalues, the transformations which lead to the largest reduction in the dimension of $\underline{\underline{T}}$, are f-step translations in the transverse direction. Such translations have the period $L=N/f$.

The configurations $|S\rangle$ can be assigned to sets I, which are invariant under U_L. The number of configurations in the Ith invariant set is $N_I \le L$. We can relabel the configurations in terms of the sets to which they belong, and denote them as

$$|I;j\rangle = U_L^{j-1}|I;1\rangle\ ,\quad j=1,\ldots,N_I\ . \tag{A1}$$

Here $|I;1\rangle$ is an arbitrarily chosen representative element of the Ith set, from which the other elements are generated by repeated application of the transformation U_L.

From the members of the Ith set we construct eigenstates of U_L, defined by

$$U_L|I^{(n)}\rangle = e^{i(2\pi/L)n}|I^{(n)}\rangle\ , \tag{A2}$$

where

$$n=\begin{cases} -\frac{1}{2}L+1,\ldots,0,\ldots,\frac{1}{2}L & \text{for } n \text{ even} \\ -\frac{1}{2}L+\frac{1}{2},\ldots,0,\ldots,\frac{1}{2}L-\frac{1}{2} & \text{for } n \text{ odd}\ . \end{cases}$$

The eigenvectors $|I^{(n)}\rangle$ are given by

$$|I^{(n)}\rangle = \frac{\delta(nN_I/L,\text{int})}{(N_I)^{1/2}} \times \sum_{j=1}^{N_I} e^{-i(2\pi/L)n(j-1)}U_L^{j-1}|I;1\rangle\ , \tag{A3}$$

where $\delta(nN_I/L,\text{int})=1$ if nN_I/L is an integer, and vanishes otherwise. It is easily shown that the set $\{|I^{(n)}\rangle\}$ forms a complete, orthonormal basis for the vector space spanned by the configuration $\{|S\rangle\}$.

Now consider an arbitrary operator $A^{(s)}$, which has a definite symmetry under the transformation U_L,

$$U_L^\dagger A^{(s)}U_L = e^{i(2\pi/L)s}A^{(s)}\ . \tag{A4}$$

Here $U_L^\dagger = U_L^{-1}$ is the Hermitian conjugate of U_L. The matrix elements of $A^{(s)}$ between the eigenstates $|I^{(n)}\rangle$ of U_L are

$$\begin{aligned}\langle I^{(n)}|A^{(s)}|K^{(m)}\rangle &= e^{-i(2\pi/L)s}\langle I^{(n)}|U_L^\dagger A^{(s)}U_L|K^{(m)}\rangle \\ &= e^{i(2\pi/L)(m-n-s)}\langle I^{(n)}|A^{(s)}|K^{(m)}\rangle\ .\end{aligned} \tag{A5}$$

Thus

$$\langle I^{(n)}|A^{(s)}|K^{(m)}\rangle = 0 \text{ if } (m-n-s)/L \neq \text{integer}\ . \tag{A6}$$

The transfer matrix $\underline{\underline{T}}$ is a special case of an operator $A^{(0)}$, invariant under U_L, so

$$\langle I^{(n)}|\underline{\underline{T}}|K^{(m)}\rangle = \delta_{m,n}\langle I^{(n)}|\underline{\underline{T}}|K^{(n)}\rangle\ , \tag{A7}$$

which simply restates the fact that $\underline{\underline{T}}$ is block diagonal in the basis $\{|I^{(n)}\rangle\}$. The nonvanishing matrix elements are given explicitly as[11]

$$\begin{aligned}{}^{(n)}T_{IK} &\equiv \langle I^{(n)}|\underline{\underline{T}}|K^{(n)}\rangle \\ &= \delta(nN_I/L,\text{int})\delta(nN_K/L,\text{int})\frac{(N_IN_K)^{1/2}}{P} \\ &\quad\times \sum_{j=1}^{P} e^{-i(2\pi/L)n(j-1)}\langle I;1|\underline{\underline{T}}U_L^{(j-1)}|K;1\rangle\ ,\end{aligned} \tag{A8}$$

where P is the largest common denominator of N_I and N_K.

Any adsorbate phase which may be reached by a second-order phase transition is described by the D wave vectors $\vec{k}_i$, which generate a D-dimensional irreducible representation of the full symmetry group of the substrate lattice.[13] The D-component order parameter characterizing such a phase is

$$\psi_{\vec{k}_i} = \frac{1}{MN}\sum_{\vec{r}}\sigma(\vec{r})\cos(\vec{k}_i\cdot\vec{r})\ ,\quad i=1,\ldots,D \tag{A9}$$

where the sum extends over all sites $\vec{r}$ of the lattice, and MN is the total number of sites. In transfer-matrix calculations the lattice is partitioned into a one-dimensional array of M layers, each containing N sites. When the lattice is partitioned in this way, the global order parameter $\psi_{\vec{k}_i}$ can be decomposed into a sum of single-layer order parameters,

$$\begin{aligned}\psi_{\vec{k}_i} &= \frac{1}{M}\sum_{m=1}^{M}\frac{1}{N}\sum_{n=1}^{N}\sigma(\vec{r}(m,n))\cos[\vec{k}_i\cdot\vec{r}(m,n)] \\ &\equiv \frac{1}{M}\sum_{m=1}^{M} c_m\psi_{\vec{k}_i}(S_m)\ .\end{aligned} \tag{A10}$$

The single-layer order parameters $\psi_{\vec{k}_i}(S_m)$ depend on m only through the single-layer configurations S_m. Their symmetry under the translation U_L is determined by $\vec{k}_i$.

The symmetry group of the centered rectangular lattice considered in this work is $C2mm$. The (2×1) phase is described by the two wave vectors which join the center of the Brillouin zone to its long faces. The two components of the associated order parameter are

$$\psi_{(2\times1)}=\frac{1}{M}\sum_{m=1}^{M}(-1)^m\psi_{(2\times1)}(m) \tag{A11a}$$

and

$$\psi_{(1\times2)}=\frac{1}{M}\sum_{m=1}^{M}(-1)^m\psi_{(1\times2)}(m)\ , \tag{A11b}$$

where the single-layer order parameters are

$$\psi_{(2\times1)}(m)=\frac{1}{N}\sum_{p=1}^{N/2}(-1)^{p-1}(\sigma_{m,2p-1}-\sigma_{m,2p}) \tag{A12a}$$

and

$$\psi_{(1\times2)}(m)=\frac{1}{N}\sum_{p=1}^{N/2}(-1)^{p-1}(\sigma_{m,2p-1}+\sigma_{m,2p})\ . \tag{A12b}$$

Both of these are antisymmetric under the two-step transverse translation which leaves the lattice and Hamiltonian invariant. The $(2\times2)_{3/4}$ phase is a linear combination of the (2×1) and (1×2) phases. The disordered phase is described by the wave vector $\vec{0}$, which generates the identity representation of the lattice symmetry group. The associated order parameter is

$$\psi_0=\frac{1}{M}\sum_{m=1}^{M}\psi_{\rm FM}(m)\ , \tag{A13}$$

where the "ferromagnetic" single-layer order parameter

$$\psi_{\rm FM}(m)=\frac{1}{N}\sum_{n=1}^{N}\sigma_{m,n} \tag{A14}$$

is symmetric under the two-step transverse translation.

The correlation function for a single-layer order parameter ψ is[11]

$$\Gamma_\psi(m)=\sum_{\beta>1}|\psi_{1\beta}|^2\left[\frac{\lambda_\beta}{\lambda_1}\right]^m + \sum_{\gamma}\langle 1|\psi^\dagger\mathscr{P}_\gamma\psi|1\rangle\left|\frac{\lambda_\gamma}{\lambda_1}\right|^m\cos(m\phi_\gamma)\ . \tag{A15}$$

Here the λ_β are the purely real, nondegenerate eigenvalues of $\underline{\underline{T}}$ and $\lambda_{\gamma\pm}=|\lambda_\gamma|\exp(\pm i\phi_\gamma)$ are the complex-conjugate pairs of eigenvalues. The operator $\mathscr{P}_\gamma=|\gamma+\rangle\langle\gamma+|+|\gamma-\rangle\langle\gamma-|$ is the projection operator onto the subspace spanned by the eigenvectors $|\gamma+\rangle$ and $|\gamma-\rangle$.

From the above discussion of the block diagonalization of $\underline{\underline{T}}$ it follows that each eigenvector $|\alpha\rangle$ of $\underline{\underline{T}}$ is also an eigenvector of U_L,

$$\underline{\underline{T}}\,|\alpha\rangle=\lambda_\alpha|\alpha\rangle$$

and (A16)

$$U_L|\alpha\rangle=e^{i(2\pi/L)n_\alpha}|\alpha\rangle\ .$$

Thus n_α specifies the eigenvalue of U_L in the subspace $\{|I^{(n_\alpha)}\rangle\}$ to which $|\alpha\rangle$ belongs. In other words,

$$|\alpha\rangle=\sum_I|I^{(n_\alpha)}\rangle\langle I^{(n_\alpha)}|\alpha\rangle\ . \tag{A17}$$

In particular it can be shown that the eigenvector $|1\rangle$, corresponding to the largest eigenvalue λ_1, belongs to the symmetric subspace, i.e., $n_1=0$. The matrix elements $\psi_{1\beta}$ which occur in the correlation function $\Gamma_\psi(m)$ are therefore given by

$$\psi^{(s)}_{1\alpha}=\sum_{I,K}\langle 1|I^{(0)}\rangle\langle I^{(0)}|\psi^{(s)}|K^{(n_\alpha)}\rangle\langle K^{(n_\alpha)}|\alpha\rangle =\delta_{s,n_\alpha}\sum_{I,K}\langle 1|I^{(0)}\rangle\langle I^{(0)}|\psi^{(n_\alpha)}|K^{(n_\alpha)}\rangle\langle K^{(n_\alpha)}|\alpha\rangle\ . \tag{A18}$$

We thus can determine whether $\psi^{(s)}_{1\beta}$ vanishes by symmetry without knowing the detailed expansion of $|\beta\rangle$. The eigenstates $|\gamma+\rangle$ and $|\gamma-\rangle$ have the same symmetry under the symmetry operation U_L. The same symmetry arguments therefore apply to the terms $\langle 1|\psi^\dagger\mathscr{P}_\gamma\psi|1\rangle$ as to the terms $|\psi_{1\beta}|^2$.

*Present address: Department of Mechanical Engineering, State University of New York at Stony Brook, Stony Brook, NY 11794.

†Present address: Physics Department, Tampere University of Technology, P.O. Box 527, Tampere 10, Finland.

[1]L. D. Roelofs and P. J. Estrup, Surf. Sci. 125, 51 (1983).

[2]M. G. Lagally, T.-M. Lu, and G.-C. Wang, in *Ordering in Two Dimensions,* edited by S. Sinha (Elsevier, New York, 1980).

[3]G.-C. Wang, T. M. Lu, and M. G. Lagally, J. Chem. Phys. 69, 479 (1978).

[4]G. B. Blanchet, P. J. Estrup, and P. J. Stiles, J. Vac. Sci. Technol. 18, 502 (1981).

[5]K. Binder and D. P. Landau, Phys. Rev. B 21, 1941 (1980); Surf. Sci. 108, 503 (1981).

[6]L. D. Roelofs, in *Chemistry and Physics of Solid Surfaces IV,* Vol. 20 of *Springer Series in Chemical Physics,* edited by R. Vanselow and R. Howe (Springer, Berlin, 1982).

[7]W. Y. Ching, D. L. Huber, M. G. Lagally, and G.-C. Wang, Surf. Sci. 77, 550 (1978); W. Y. Ching, D. L. Huber, M. Fishkis, and M. G. Lagally, J. Vac. Sci. Technol. 15, 653 (1978); E. D. Williams, S. L. Cunningham, and W. H. Weinberg, J. Chem. Phys. 68, 4688 (1978).

[8]M. P. Nightingale, Physica 83A, 561 (1976); Phys. Lett. 59A, 486 (1977); Ph.D. thesis, University of Amsterdam, 1978; Proc. K. Ned. Akad. Wet. Ser. B 82, 235 (1979).

[9]W. Kinzel, W. Selke, and K. Binder, Surf. Sci. 121, 13 (1983); W. Selke, K. Binder, and W. Kinzel, *ibid.* 125, 74 (1983).

[10]K. Kaski, W. Kinzel, and J. D. Gunton, Phys. Rev. B 27, 6777 (1983).

[11]P. A. Rikvold, Ph.D. thesis, Temple University, 1983. This thesis contains a more detailed discussion of the exponent calculations.

[12]T. L. Einstein, Surf. Sci. Lett. 84, L497 (1979).

[13]E. Domany, M. Schick, J. S. Walker, and R. B. Griffiths, Phys. Rev. B 18, 2209 (1978).

[14]C. Domb, Adv. Phys. 9, 149 (1960).

[15]P. A. Rikvold, W. Kinzel, J. D. Gunton, and K. Kaski, Phys. Rev. B 28, 2686 (1983).
[16]V. Privman and M. E. Fisher, J. Stat. Phys. 33, 385 (1983).
[17]R. B. Griffiths and B. Widom, Phys. Rev. A 8, 2173 (1973).
[18]I. D. Lawrie and S. Sarbach, in *Phase Transitions and Critical Phenomena,* edited by C. Domb and J. L. Lebowitz (Academic, London, in press).
[19]H. W. J. Blöte and M. P. Nightingale, Physica (Utrecht) 112A, 405 (1982); J. L. Cardy and P. Nightingale, Phys. Rev. B 27, 4256 (1983).
[20]P. Kleban and C.-K. Hu (unpublished); P. H. Kleban and G. Akinci, Phys. Rev. Lett. 51, 1058 (1983).